

Collective ECM remodeling organizes 3D collective cancer invasion

Jihan Kim*,¹ Yu Zheng*,² Amani A. Alobaidi*,¹ Hanqing Nan,³ Jianxiang Tian,^{4,3} Yang Jiao,^{3,2,†} and Bo Sun^{1,‡}

¹*Department of Physics, Oregon State University,
301 Weniger Hall, Corvallis, OR, USA, 97331-6507*

²*Department of Physics, Arizona State University, Tempe, AZ 85287-6106*

³*Materials Science and Engineering, Arizona State University, Tempe, AZ 85287-6106*

⁴*Department of Physics, Qufu Normal University, Qufu 273165, China*

Tumor metastasis, traditionally considered as random spreading of individual cancer cells, has been shown to also involve coordinated collective invasion in the tissue space. Here we demonstrate experimentally and computationally that physical interactions between cells and extracellular matrix (ECM) support coordinated dissemination of cells from tumor organoids. We find that collective remodeling of the ECM fibrous structure by cell-generated forces produces reciprocal cues to bias cell motility. As a result, dissemination of cells from tumor organoids are controlled by the organoid geometry. Our results indicate that mechanics and geometry are closely coupled in multicellular processes during metastasis and morphogenesis. This study also suggests that migrating cells in 3D ECM represent a distinct class of active particle system where the collective dynamics is governed by the micromechanical remodeling of the environment rather than direct particle-particle interactions.

Collective invasion of cancer cells plays an important role in the lethal metastasis of tumors [1, 2]. However, the mechanisms that coordinate 3D collective cell motility is not fully understood. A number of mechanisms have been shown to coordinate multicellular invasion. For instance, cell-cell adhesion leads to group invasion as cell clusters [3, 4]. Strands of cells may follow each other along microtracks created by leader cells [5, 6]. Communications mediated by diffusive factors have also been shown to coordinate the collective motility of tumor cells by establishing leader-follower phenotypes [7].

Here we propose and test a distinct mechanism for 3D collective invasion that only depends on the physical interactions between cancer cells and their ECM (extracellular matrix). We show both experimentally and computationally that the reconfigurability of ECM, as well as the force generation and force sensation of cancer cells maintain a mechanical conversation between invading tumor cells in 3D tissue space. As a result, the collective invasion is coordinated by collective micromechanical remodeling of the ECM, which leads to organoid-geometry dependent dissemination of the tumor cells. Our results suggest that ECM-mediated physical interactions between invasive cells may play a powerful role in determining the metastatic potential of malignant tumors.

Geometry controls tumor organoid invasiveness and collective micromechanical remodeling of ECM. To study the 3D collective invasion of cancer cells, we use tumor organoid models created with DIGME technique [8]. Each organoid consists of approximately 1000 GFP-labeled MDA-MB-231 cells molded into various shapes in 3D type I collagen ECM (Fig. S1). Confocal imaging starts immediately after the gelation process

completes (time zero).

We first compare tumors of two different cross-sectional geometries: circular and triangular. In particular, we measure the invasion depths Δd as the distance between the outer boundaries of the tumors at day 0 and day 10 as shown in Fig. 1(a-b). The circular tumors disseminate rapidly, with the mean invasion depth to be more than 500 μm . The triangular tumors, on the other hand, disseminate much slower. The invasion depths measured in the edge and tip directions are both around 200 μm , less than half of the mean invasion depth of circular tumors (Fig. 1c).

The cells in the organoids are harvested from the same subculture, and the invasion assays are maintained in the same tissue culture conditions, it is very unlikely that circular tumors and triangular tumors consists of two distinct phenotypes. Ruling out single-cell sources, Fig. 1c suggests the 3D invasion of a tumor organoid is a complex multicellular phenomenon, where cell-cell and cell-ECM interactions may play important roles.

We first note that there are rarely any cell-cell adhesions during the invasion process due to the highly mesenchymal nature of MDA-MB-231 cells. In distinction from cells exhibiting epithelial features, MDA-MB-231 cells characteristically disseminate as isolated individuals (Fig. 1d). We then consider the possibility of indirect cell-cell interactions. Previously we reported that the traction forces from cell pairs create aligned collagen fiber bundles, such that the remodeled ECM provides a potential channel to mediate mechanical communications between cancer cells [9]. For an disseminating tumor organoid, the micro-mechanical remodeling of the ECM could be even stronger due to additive effects. Therefore, we hypothesize that collective cell remodeling of the ECM renders the invasion of tumor organoids to depend on organoid geometry.

To test this hypothesis, we first examine if the ECM deformation caused by tumor-generated mechanical forces depends on the tumor geometry. We embed 1- μm di-

*These authors contributed equally to this work.

†correspondence sent to: yang.jiao.2@asu.edu

‡correspondence sent to: sunb@onid.orst.edu

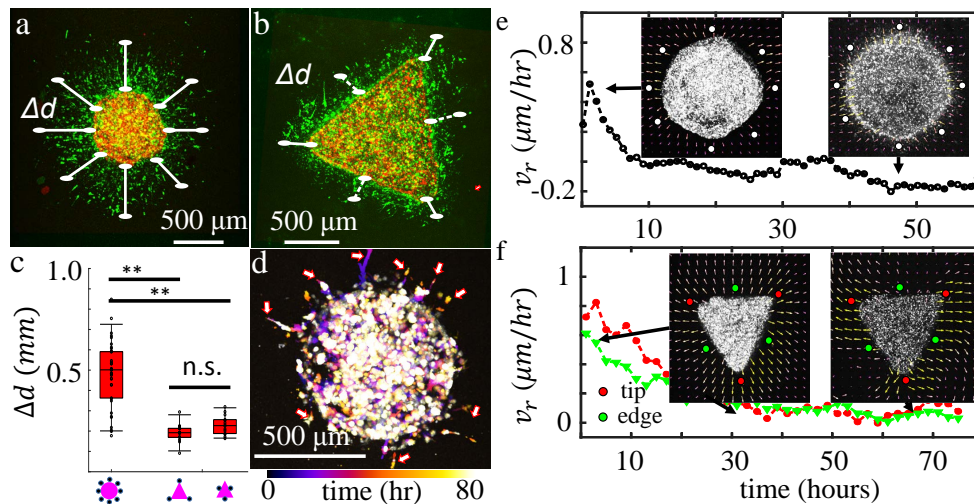


FIG. 1: Geometry controls tumor organoid invasiveness and ECM remodeling. (a-b) Tumor organoid morphology shown by maximum projection at day 0 (red) and day 10 (green). For a circular tumor the invasion depth Δd is measured along eight equally spaced angles (a). For a triangular tumor Δd is measured along tip and edge directions separately (b). (c) The invasion depths of circular and triangular tumors. $N = 5$ tumors were measured for each geometry. Statistical comparison are done with t-test. **: $p < 0.01$. n. s. : not significant. (d) Time-coded image projection showing the invasion process of a circular MDA-MB-231 organoid. The cells disseminate individually (arrows) with little contact after leaving the organoid. (e-f) The average radial velocity of the ECM deformation near expanding tumors. In (e) the velocity is averaged over the 8 dotted locations shown in the inset. In (f) the velocity is averaged over the dotted locations along the edge and tip directions respectively. Insets in (e-f) show the net deformation of the ECM at two time points (black arrows).

ameter fluorescently-labeled polystyrene particles in the collagen ECM and use particle image velocimetry (PIV) to quantify the ECM deformation field. Fig. 1 (e-f) show the radial velocity v_r of the ECM by averaging over symmetric locations (dotted points in the insets of Fig. 1 (e-f)). A circular tumor first pushes out the ECM ($v_r > 0$) due to cell spreading upon seeding (leading to overall expansion of the organoid), then pulls in the ECM ($v_r < 0$) with their traction force. As a result, after 2 days the ECM shows net inward deformation while some of the cells have already been disseminated from the tumor (Fig. 1e insets). On the other hand, we find that a triangular tumor mostly pushes out the ECM, albeit with a diminishing rate. As a result, the ECM surrounding the triangular tumor maintains a radially outward net deformation (Fig. 1f).

Computational modeling of collective micromechanical remodeling of ECM and tumor invasion. To gain further insights on how collective ECM remodeling modulates the collective cancer invasion, we devise a multi-scale computational model that takes into account the fibrous microstructure of the ECM [10], nonlinear ECM mechanics [11], as well as cell motility directed by contact guidance cues [12, 13].

Based on the experimental observations, we consider the dissemination of tumor organoids to start from an expansion phase, where cells spread and push out the ECM. This is followed by an invasion phase, where cells pull in the ECM and migrate. We model tumor cells as polarized active particles with coupled force generation and locomotion [12] (Fig. S2-S7). Cells deform the ECM

fibers in their vicinity, which in turn alters the migration and polarization of the cells. Explicitly accounting for the reciprocal interactions between cells and ECM allows us to investigate the collective migration regulated by the non-local mechanical dialogues among the cells mediated by the ECM.

We first employ the computational model to simulate and calculate the remodeling of the ECM surrounding circular and triangular tumor organoids. Fig. 2 (a-b) show the relative magnitudes of displacement fields in the ECM, where the maximum value is normalized to 1. Here we measure the ECM properties at 5 hours and 50 hours, two time points empirically determined to represent the expansion and invasion phases respectively. The magnitude of displacement decays roughly as $1/r^3$ as one moves away from the organoids. After the expansion phase, individual cells migrate away from the original organoid. The right panels of Fig. 2(a-b) show locations of the invaded cells in a typical simulation run. Cell invasion is accompanied with continuous ECM deformation. As shown in Fig. 2(c-d), our simulated ECM radial velocity agree well (qualitatively for circular organoids and quantitatively for triangular organoids) with experimental measurements. Importantly, the contractile deformation is much more pronounced near circular tumors compared with triangular tumors.

To better reveal the structural remodeling of the ECM, we have calculated the average orientation of the ECM fibers with respect to the tangential direction of the tumor surfaces (Fig. 2e-f). During the expansion phase, organoids push the fibers to be aligned parallel to the

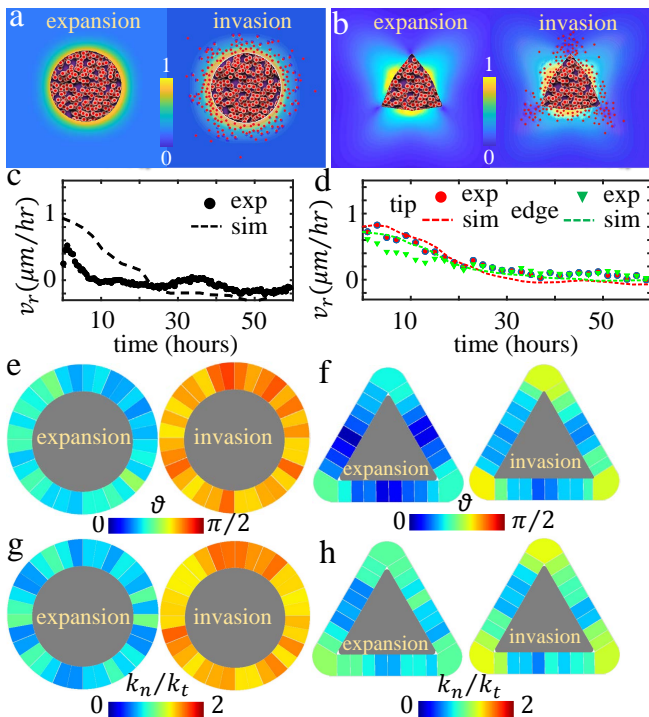


FIG. 2: Simulated ECM remodeling by circular and triangular tumor organoids. (a-b) The magnitudes of ECM displacement fields at 5 hours (representing the expansion phase) and at 50 hours (representing invasion phase) of circular and triangular organoids. Maximum deformation is normalized to 1. (c-d) Radial velocities of the ECM sampled near circular and triangular organoids at locations corresponding to the experimental measurements in Fig. 1(e-f). Abbreviations: exp: experiment; sim: simulation. (e-f) The orientation of ECM fibers near the organoids at 5 hours (expansion) and at 50 hours (invasion). θ is measured as the average angle of fibers with respect to their local tangential direction of the tumor boundary. (e-f) The micromechanical anisotropy defined as k_n/k_t at 5 hours (expansion) and at 50 hours (invasion). k_n and k_t are the micromechanical stiffness along the normal direction and tangential direction of the tumor boundary respectively. See Fig. S8 for more details. In (e-h) we sample $100 \mu\text{m}^3$ volume elements next to the organoids to obtain the average fiber orientations and stiffness ratios.

tumor boundary, which bias the cell polarization accordingly. Later on, the pulling forces from the cells reorient the fibers. For circular tumors, the collective cellular traction force is sufficient to align the ECM fibers radially (Fig. 2e), contributing to the accelerated dissemination. In contrast, the fibers remain tangentially aligned along the flat edges of the triangular tumors (Fig. 2f).

The structural remodeling of the ECM significantly reconfigures the micromechanics of the ECM. We find that for both circular and triangular tumors ECM is consistently stiffer in the direction of fiber alignment, and softer in the direction perpendicular to the fibers. Such mechanical cues may further regulate the dynamics and functions of cells through mechanosensing pathways [14].

Our simulations show that the circular tumors exhibit

larger invasion depths compared with the triangular tumors (Fig. S9), which is consistent with the experimental observations. To further explore the mechanisms behind the geometry-dependent collective migration, we modified the simulation parameters to steer the cell-ECM interactions. We find that when the cell polarization and ECM fiber orientations become uncorrelated, the invasion depth of tumors drastically reduces (Fig. S10). This is consistent with the experimental results that reducing the level of contact guidance diminished the advantage of circular tumors in dissemination (Fig. S11). We also find that reducing the cellular traction forces leads to weaker ECM remodeling, and thus weaker dependence of tumor invasion dynamics on the organoid geometry (Fig. S12).

Collective invasion of tumor organoids with complex shapes. Having tested our simulation model against experimental results for circular and triangular tumors, we ask if the mechanical principles considered in our model are sufficient to predict the invasiveness of tumors with more complex geometries. We focus on two particular shapes of tumors: semicircle and star. The boundary of a semicircle contains regions of both positive and zero curvature, therefore can be considered to be a hybrid of circular and triangular tumors. A star shape, on the other hand, contains both convex and concave surfaces.

Taking into account of the asymmetric shape of semicircle diskoids, we divide the ECM space into cap, corner and flat regions (Fig. 3a). We manually identify all disseminated cells and their locations after 10 days from seeding the original tumor. To help visualize the spatial distribution of the cells we compute the normalized cell density ρ_N (Methods), which represents a dilution factor: if $\rho_N = 1$ then the local cell density is the same as in the original tumor, where all cells are presumably uniformly distributed in the original tumor.

We find the cell density is almost uniform surrounding the original semicircle diskoid, and decreases rapidly at larger distance. However, the flat region contains fewer cells that migrate deeply into the ECM space from the diskoid boundary. To further quantify the relation between invasiveness and local geometry of tumors, we calculate the ranked average invasion depths (RAID) $\Delta\bar{D}(f)$. In particular, we first measure the invasion depth Δd_i of each cell i as the distance of the cell from the original tumor boundary (arrows in Fig. 3a,b). We then compute $\Delta\bar{D}(f)$ as the average invasion depth of cells in the top f percentile ranked by Δd_i . Using the metric RAID, we compare the invasiveness of cells in each of the three regions of the ECM surrounding semicircle diskoids. As shown in Figure. 3c, cells in the cap region are leading the dissemination. For instance, the top 10% invaders in the cap region have an average invasion depth of $672 \mu\text{m}$, while the top 10% invaders in the corner and flat region have an average invasion depth of $470 \mu\text{m}$. At a percentile of 5%, cells in the cap region have a lead of $200 \mu\text{m}$ than cells in the flat region.

Consistent with the previous observations in Fig. 1,

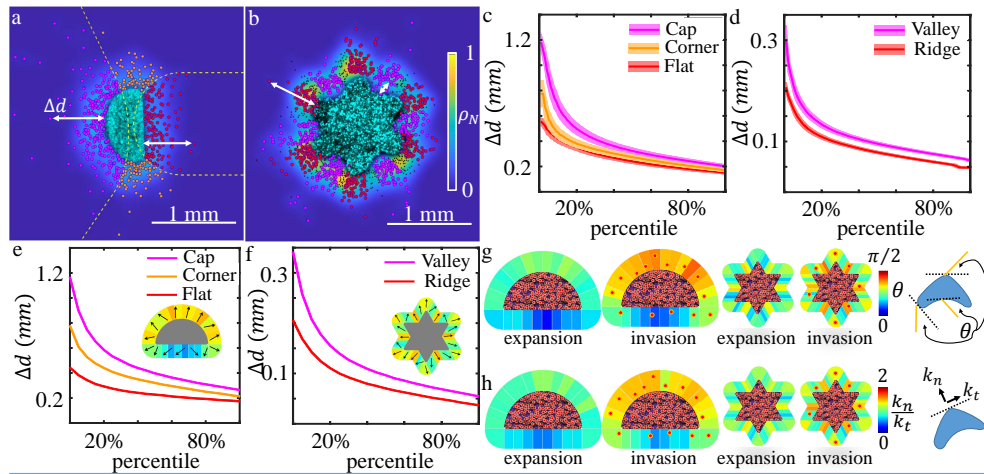


FIG. 3: Collective invasion of tumor organoids with complex shapes. (a-b) Snapshots of semicircle and star-shaped diskoids at day 10 and day 3 respectively. The images of the organoids at day zero are surrounded by the normalized cell density ρ_N (see methods for definition). Dots represent locations of all the disseminated cells experimentally observed for each tumor shape. In (a) the ECM space is divided into cap, corner and flat regions separated by the yellow dashed curves. In (b) the ECM space is divided into ridge and valley regions. Cells in different regions are labeled with different colors. The invasion depth Δd of a cell is the distance between the cell and the boundary of the organoid at day zero (white arrows show examples). (c-d) Ranked average invasion depths (RAID) of semicircle and star-shaped diskoids. The solid lines and shaded areas represent the means and standard deviations obtained from 500 bootstraps. In (a-d) approximately 1000 disseminated cells are identified and included in the statistics from $N=4$ (semicircle diskoid) and $N=5$ (star diskoid) biological replicas respectively. (e-f) Simulated RAID profiles for semicircle and star shaped tumors. Insets: magnitude (heatmap, normalized by maximum), and direction (arrows) of average cell velocity near the tumor organoids. (g-h) The simulated average fiber orientation and micromechanical anisotropy in a layer of $\sim 100\mu\text{m}$ surrounding the tumors after the expansion and invasion phases. Here θ is defined as the acute angle between a fiber and the local tangential direction of the tumor boundary, while k_n and k_t are defined previously (Fig. S8).

the invasiveness of semicircular diskoids provides strong evidence that local geometry regulate cancer cell dissemination. In particular, a positive curvature in the tumor surface accelerates the overall invasion [15].

We have also quantified the invasiveness of star-shaped diskoids after 3 days of seeding the tumor. In particular, we divide the ECM space into regions that are in the direction of the tips (positive curvature), and regions that are in the direction of valleys (negative curvature). Cells in the buffer regions (black dots in Fig. 3b) are excluded from the analysis.

By measuring RAID we find that overall cells in the valley region possess larger invasion depth (Fig. 3d), suggesting that negative curvature accelerates cell dissemination even more than positive curvature. Of note, at 10 days, the disseminated cells become uniformly distributed in all directions. This is due to the proximity of the ridge and valley regions as well as the mixing caused by lateral motion of the cells,

These experimental results agree well with the predictions of our simulations as shown in Fig. 3e and f. Furthermore, our simulations also reveal the ECM remodeling by the tumor organoids. Fig. 3(g-h) shows the average fiber orientation and microscopic anisotropy in the expansion and invasion phases. For semicircle organoids, fibers in the flat region remain tangentially aligned to the tumor boundary through the whole process; whereas

fibers in the cap region are re-oriented radially by cellular traction force during the invasion phase. For star-shaped organoids, fiber orientation in the ridge region rotates from tangential of the tumor boundary to random alignment; whereas fibers in the valley region are pulled normal to the tumor boundary during the invasion phase. The structural anisotropy translates directly to the micromechanical anisotropy, such that the ECM is stiffer in the direction parallel to the fiber alignment. These results confirm that local geometry program collective force generation and ECM remodeling by the cancer cells, which modulates the rate of dissemination of the tumors.

In this letter, we demonstrate a previously unrecognized mechanism of cell-cell interaction that coordinates multicellular dynamics. This mechanism does not require direct contact between cells such as cadherin-based adhesion [3, 4] or contact inhibition [16, 17], nor it relies on the cooperation of leader-follower phenotypes [5, 6, 18, 19]. Instead, we show both experimentally and computationally that cells collectively apply forces to their ECM [20], which in turn provides mechanical cues to bias cell motility. Because collective force generation can be controlled by geometry, we find dissemination of cancer cells from tumor organoids are dependent on tumor geometry.

Our results provide physical insights for processes in cancer biology and morphogenesis. Clinical studies have

shown that collagen fibers aligned tangentially and normally to tumor boundary correspond to opposite prognosis [21, 22]. While the origin of tumor-associated ECM misalignment is unclear, our results suggest that tumor geometry is an important contributing factor. On the other hand, mesenchymal cell migration is often considered as a single-cell process during development and diseases [23, 24]. Our model system show that underlying multicellular coordination may take place in the form of collective force generation and ECM remodeling. Together, we find that 3D collective cell migration may exploit the mechanical feedback between force-generating cells and reconfigurable ECM as an indirect yet effective channel of communication .

Finally, our results show that 3D migrating cells represent a distinct class of active particles which actively re-sculpture their microenvironment and respond to the cues generated by themselves and others. Future research is needed to systematically investigate the collective dynamics of such active particles as a route to understand general living systems.

Methods

Sample preparation. See Supplementray Information for details.

Image analysis. Confocal images were taken using Leica SPE at a rate of 30 min per frame for continuous imaging or at days 0, 1, 3, 5, 10 for discrete imaging. Cell locations were projected onto the $x - y$ plane, whereas movement in the z direction is relatively small [8]. The invasion depths were manually measured with the help of NIH ImageJ. The deformation of the ECM was measure using PIVlab implemented on Matlab. To calculate the velocity field in the ECM we perform PIV analysis on image pairs with 2-hour delay.

To approximate the cell density from the scattered cell locations we use a gaussian kernel:

$$\rho_N(\mathbf{r}) = \frac{A_0}{m} \sum_{i=1}^m \frac{1}{2\pi\sigma^2} e^{-\frac{(\mathbf{r}-\mathbf{r}_i)^2}{2\sigma^2}} \quad (1)$$

Here we choose the kernel width σ to be $80 \mu\text{m}$, approximately twice the size of a cell. m is the total number of disseminated cells, and A_0 is the area of the original tumor diskoid. To calculate the ranked average invasion depth (RAID) we used the Matlab `quantile()` function to select the data for averaging.

Computation. See supplementary information for details.

Data Availability

All data and computer codes are available from the authors upon reasonable request.

Acknowledgment

The research is supported by a Scialog Program sponsored jointly by Research Corporation for Science Advancement and the Gordon and Betty Moore Foundation through a grant to Oregon State University by the Gordon and Betty Moore Foundation. B. S. is partially supported by the Medical Research Foundation of Oregon and SciRIS-II award from Oregon State University. J. K. is partially supported by the National Science Foundation grant PHY-1400968.

Author Contributions

B. S. and Y. J. designed the research and oversaw the experimental and computational studies respectively. J. K., Y. Z., A. A., H. N., J. T. collected data. All authors analyzed data and wrote the manuscript. Y. Z. and H. N. thank Arizona State University for the University Graduate Fellowship.

-
- [1] P. Friedl, J. Locker, E. Sahai, and J. E. Segall. Classifying collective cancer cell invasion. *Nat. Cell Biol.*, 14(7):777–783, 2012.
- [2] Vincent Hakim and Pascal Silberzan. Collective cell migration: a physics perspective. *Reports on Progress in Physics*, 80(7):076601, 2017.
- [3] KJ Cheung, E Gabrielson, Z Werb, and AJ Ewald. Collective invasion in breast cancer requires a conserved basal epithelial program. *Cell*, 155(7):1639, 2013.
- [4] Nicola Aceto, Aditya Bardia, David.T. Miyamoto, Maria.C. Donaldson, Ben.S. Wittner, Joel.A. Spencer, Min Yu, Adam Pely, Amanda Engstrom, Huili Zhu, Brian.W. Brannigan, Ravi Kapur, Shannon.L. Stott, Toshi Shioda, Sridhar Ramaswamy, David.T. Ting, Charles.P. Lin, Mehmet Toner, Daniel.A. Haber, and Shyamala Maheswaran. Circulating Tumor Cell Clusters Are Oligoclonal Precursors of Breast Cancer Metastasis. *Cell*, 158(5):1110–1122, 2014.
- [5] Katarina Wolf, Yi I. Wu, Yueying Liu, Jörg Geiger, Eric Tam, Christopher Overall, M. Sharon Stack, and Peter Friedl. Multi-step pericellular proteolysis controls the transition from individual to collective cancer cell invasion. *Nature Cell Biology*, 9(8):893–904, 2007.
- [6] Cedric Gaggioli, Steven Hooper, Cristina Hidalgo-Carcedo, Robert Grosse, John F. Marshall, Kevin Harrington, and Erik Sahai. Fibroblast-led collective invasion of carcinoma cells with differing roles for RhoGTPases in leading and following cells. *Nature Cell Biology*,

- 9(12):1392–1400, 2007.
- [7] J Konen, E Summerbell, B Dwivedi, K Galior, Y Hou, L Rusnak, A Chen, J Saltz, W Zhou, L H Boise, P Vertino, L Cooper, K Salaita, J Kowalski, and A I Marcus. Image-guided genomics of phenotypically heterogeneous populations reveals vascular signalling during symbiotic collective cancer invasion. *Nat. Comm.*, 8:15078, 2017.
- [8] A. A. Alobaidi and B. Sun. Probing three-dimensional collective cancer invasion with digme. *Cancer Convergence*, accepted, 2017.
- [9] J. Kim, J. Feng, C. A. R. Jones, X. Mao, L. M. Sander, H. Levine, and B. Sun. Stress-induced plasticity of dynamic biopolymer networks. *Nature Communications*, 2017, in press.
- [10] C. A. Jones, L. Liang, D. Lin, Y. Jiao, and B. Sun. The spatial-temporal characteristics of type I collagen-based extracellular matrix. *Soft Matter*, 10(44):8855–8863, 2014.
- [11] J Steinwachs, C Metzner, K Skodzek, N.Lang, I Thievensen, C Mark, S Münster, K E Aifantis, and B Fabry. Three-dimensional force microscopy of cells in biopolymer networks. *Nat. Methods*, 13:171, 2016.
- [12] Weijing Han, Shaohua Chen, Wei Yuan, Qihui Fan, Jianxiang Tian, Xiaochen Wang, Longqing Chen, Xixiang Zhang, Weili Wei, Ruchuan Liu, et al. Oriented collagen fibers direct tumor cell intravasation. *Proceedings of the National Academy of Sciences*, 113(40):11208–11213, 2016.
- [13] Jingchen Feng, Herbert Levine, Xiaoming Mao, and Leonard M Sander. Stiffness sensing and cell motility: Durotaxis and contact guidance. *bioRxiv 320705*, 2018.
- [14] Tianzhi Luo, Krithika Mohan, Pablo A. Iglesias, and Douglas N. Robinson. Molecular mechanisms of cellular mechanosensing. *Nature Materials*, 12:10641071, 2013.
- [15] Eline Boghaert, Jason P Gleghorn, KangAe Lee, Nikolce Gjorevski, Derek C Radisky, and Celeste M Nelson. Host epithelial geometry regulates breast cancer cell invasiveness. *Proceedings of the National Academy of Sciences*, 109(48):19632–7, 2012.
- [16] Brian A Camley, Yunsong Zhang, Yanxiang Zhao, Bo Li, Eshel Ben-Jacob, Herbert Levine, and Wouter-Jan Rap-
pel. Polarity mechanisms such as contact inhibition of locomotion regulate persistent rotational motion of mammalian cells on micropatterns. *Proceedings of the National Academy of Sciences*, 111(41):14770–5, 2014.
- [17] Juliane Zimmermann, Brian A Camley, Wouter-Jan Rappel, and Herbert Levine. Contact inhibition of locomotion determines cell-cell and cell-substrate forces in tissues. *Proceedings of the National Academy of Sciences*, 113(10):2660–5, 2016.
- [18] Naoya Yamaguchi, Takeomi Mizutani, Kazushige Kawabata, and Hisashi Haga. Leader cells regulate collective cell migration via Rac activation in the downstream signaling of integrin $\beta 1$ and PI3K. *Scientific Reports*, 5:1–8, 2015.
- [19] Zachary S. Dean, Paul Elias, Nima Jamilpour, Urs Utzinger, and Pak Kin Wong. Probing 3D collective cancer invasion using double-stranded locked nucleic acid biosensors. *Analytical Chemistry*, 88(17):8902–8907, 2016.
- [20] Amani A Alobaidi, Yaopengxiao Xu, Shaohua Chen, Yang Jiao, and Bo Sun. Probing cooperative force generation in collective cancer invasion. *Physical Biology*, 14(4):045005, jun 2017.
- [21] Paolo P Provenzano, Kevin W Eliceiri, Jay M Campbell, David R Inman, John G White, and Patricia J Keely. Collagen reorganization at the tumor-stromal interface facilitates local invasion. *BMC Medicine*, 4(1):38, 2006.
- [22] M W Conklin, J C Eickhoff, K M Riching, C A Pehlke, K W Eliceiri, P P Provenzano, A Friedl, and P J Keely. Aligned Collagen Is a Prognostic Signature for Survival in Human Breast Carcinoma. *Am. J. Path.*, 178(3):1221, 2011.
- [23] Jonathan M Lee, Shoukat Dedhar, Raghu Kalluri, and Erik W Thompson. The epithelial-mesenchymal transition: new insights in signaling, development, and disease. *The Journal of cell biology*, 172(7):973–81, 2006.
- [24] Hervé Acloque, Meghan S Adams, Katherine Fishwick, Marianne Bronner-Fraser, and M Angela Nieto. Epithelial-mesenchymal transitions: the importance of changing cell state in development and disease. *The Journal of clinical investigation*, 119(6):1438–49, 2009.